IMPREGNATED MEMBRANES FOR WATER PURIFICATION USING FORWARD OSMOSIS

by

Shizhong Zhao

June 29,2015

A thesis submitted to the

Faculty of Graduate School of

The University at Buffalo, State University of New York

in partial fulfillment of the requirement for the

degree of

Master of Science

Department of Chemical and Biological Engineering

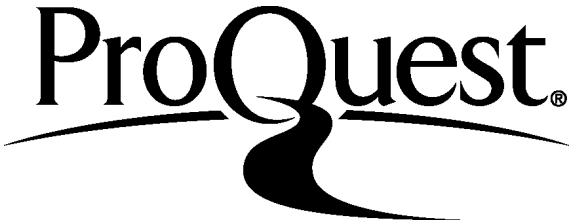

ACKNOWLEDGEMENTS

I would like to convey my gratitude to my advisor, Dr. Haiqing Lin, who brings me to the membrane world with patient guidance and constant support. His advices and directions on both academic and non-academic area are the driving force as I went through this long process.

I also would like to thank my committee member, Dr. Chong Cheng and Dr. Ning Dai for their comments on my thesis manuscript finalization.

Thank you to all the fellows in our lab such as Lingxiang Zhu and Junyi Liu. They help me with discussions on many tricky aspects of the project.

I appreciate my parents' financial support for my graduate program and their encouragement behind me. I will not make it without their support and I'm grateful for them, who offer me this great opportunity studying in the US.

LIST OF FIGURES

ABSTRACT

Forward osmosis (FO) provides an energy efficient route for seawater desalination and wastewater treatment, because water transport is driven by the osmotic pressure difference across the membrane and there is no need of feed compression. The current FO membranes are comprised of a selective layer on top of a thick microporous support and paper layer, which present significant resistance for water transport, decreasing water flux and preventing FO from wide adoption. This study investigates novel membranes consisting of a porous structure fully impregnated with a hydrophilic polymer. The elimination of the open pore structures in these impregnated membranes minimizes the effect of concentration polarization on water transport, increasing the water flux. More specifically, a series of hydrophilic polymers based on poly(ethylene glycol) diacrylate (PEGDA) were prepared and characterized for water sorption and permeation. Impregnated membranes consisting of crosslinked PEGDA in porous Solupor® supports were prepared and characterized for the water and salt transport properties using a dead-end filtration system, salt kinetic desorption experiments and an FO system. The impregnated membranes show higher performance ratio (defined as the water flux under the FO mode to that from the dead-end filtration system) compared with commercial FO membranes, which indicates the effect of concentration polarization has been reduced in these impregnated membranes.

Nomenclature

A_W	water permeance of a membrane (LMH/bar)
B	salt permeance in the membrane (cm/s)
$C_{S,P}$	salt concentration in the permeate flow (g/cm^3)
$C_{S,F}$	salt concentration in the feed (g/cm^3)
$C_{S,F}^m$	equilibrium salt concentration in the membrane surface in contact with the feed solution (g salt/cm^3 swollen polymer)
D_S	salt diffusion coefficient (cm^2/s)
gMH	salt flux, gram salt per m^2 membrane per hour
H	height of the flow channel in the permeation cell (cm)
J_S	salt flux across the membrane (gMH)
J_W	water flux across the membrane (LMH)
k_D	mass transfer coefficient in the draw solution side adjacent to the membrane (cm/s)
$k_{D,ideal}$	mass transfer coefficient in the draw solution side adjacent to the membrane, estimated using the film theory (cm/s)
k_F	mass transfer coefficient in the feed solution adjacent to the membrane (cm/s)
K_S	salt solubility in the polymer [(g salt/cm^3 swollen polymer) / (g salt/cm^3 solution)]
l	membrane thickness (cm)
L	length of the flow channel in the permeation cell (cm)
LMH	water flux, litter per m^2 membrane per hour

M_∞	salt mass in the extraction solution at equilibrium (g)
m_0	weight of a polymer sample including sol and gel (g)
m_{air}	weight of the polymer sample in the air (g)
m_{dry}	weight of the dry polymer sample (g)
m_{gel}	weight of the polymer gel (g)
m_{liquid}	weight of the polymer sample in a liquid (g)
M_t	NaCl weight in the extraction solution at time t (g)
$M_{W,S}$	molecular weight of the salt (g/mol)
m_{wet}	weight of a swollen polymer sample at equilibrium (g)
Δp	pressure difference across the membrane (bar)
p_F	pressure on the membrane feed side (bar)
p_p	pressure on the membrane permeate side (bar)
P_S	salt permeability in the membrane (cm^2/s)
P_W	pure water permeability in the membrane (cm^2/s)
R_e	Reynolds number
R_g	the gas constant (83.1 cm^3 bar/mol K)
R_S	salt rejection (%)
t	time (s)
T	temperature (K)
v_∞	flow velocity on the membrane surface (cm/s)
v_W	equilibrium volume fraction of water in the polymer
$\bar{V}_W$	molar volume of liquid water (18 cm^3/mol)
W	width of the flow channel in the permeation cell (cm)

w_{gel}	weight fraction of the gel in the polymer
w_W	water sorption in the polymer (wt.%)

Greek letter

δ	thickness of the boundary layer (cm)
v	kinetic viscosity (cm^2/s)
π_D	osmotic pressure of the draw solution (bar)
π_F	osmotic pressure of the feed solution (bar)
π_P	osmotic pressure of the membrane permeate stream (bar)
ρ_{air}	air density (g/cm^3)
ρ_{liquid}	density of a liquid (g/cm^3)
ρ_P	density of the dry polymer (g/cm^3)
ρ_W	water density (g/cm^3)

Subscript

b	bulk property
D	draw solution side of the membrane
F	feed side of the membrane
p	polymer
P	permeate side of the membrane
S	salt
W	water

TABLE OF CONTENTS

CHAPTER 1: INTRODUCTION

Water purification has received worldwide attention because of the increasing need of clean water and the limited water supply [1-3]. Polymeric membranes have been widely used in seawater desalination, concentration of landfill leachate and wastewater treatment, due to their high energy efficiency and low cost [4-6]. Forward osmosis (FO) has recently emerged as an attractive technology for water purification, partially because of the low pressure operation and thus high energy efficiency [7-11]. The core to the FO process is a membrane highly permeable to water while rejecting solutes. During the operation, water selectively permeates through the membrane from the feed solution with low osmotic pressure to a draw solution with high osmotic pressure. The draw solution must be easily processed to produce clean water, and a concentrated solution with high osmotic pressure to be recycled to the FO process. For example, the solute in the draw solutions can be ammonia carbonate (which can be easily concentrated by heat) [12] or magnetic nanoparticles (which can be concentrated by magnetic force) [13].

The FO membranes need to have high rejection rate for the solutes to maintain high osmotic pressure difference across the membrane, and high water permeance to reduce the membrane area required for the separation. Fig. 1a shows a schematic of typical thin film composite (TFC) membranes for FO water purification. The composite membranes were originally developed for reverse osmosis desalination [4,14]. The thin, dense skin layer (~0.2 μm) performs molecular separation and the hydrophobic porous bulk of the membrane (150-200 μm) provides mechanical strength, but offers no resistance to mass transport for desalination. However, the thick porous bulk presents significant transport resistance to water flux in the FO operation [15,16]. Both the microporous support and paper layer act as diffusion barriers between the selective layer and the

draw solution in the bulk, generating concentration gradients. This effect is known as concentration polarization, and it reduces the effectiveness of the draw solution and counter-flow operation [7,10,15-20]. There is a critical need to mitigate the internal concentration polarization in the porous structure to increase the water flux and thus reduce the operation cost.

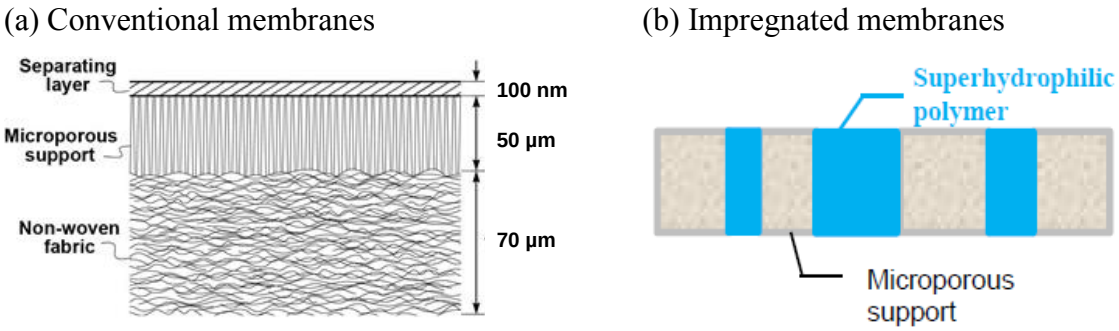

Fig. 1. (a) Schematic illustration of a conventional asymmetric thin film composite membrane used for FO water purification [10,18,19]. (b) Thin impregnated membranes (IMs).

Various approaches have been explored to minimize the water transport resistance in the support layer [21]. For example, the support and paper layer have been modified to enhance hydrophilicity by coating with hydrophilic polydopamine [20]. Membranes were prepared directly on an electron-spun nanofiber support, eliminating the thick microporous membranes [22,23]. Both approaches have improved the water flux, confirming the critical need in reducing the transport resistance in the open pores of membranes.

Another approach, to be examined in this study, is to design impregnated membranes, completely eliminating the open pore structures in the membranes. These membranes consist of a highly porous (up to 80% porosity) support matrix impregnated with a hydrophilic polymer, as shown in Fig. 1b. The porous support (10-40 µm) can be made considerably thinner than the conventional ultrafiltration membrane (100-150 µm), while providing sufficient mechanical integrity for membrane handling and operation. These impregnated membranes (IMs) were

originally developed for fuel cell membrane applications [24-31] and spacers for battery applications [32,33]. Recently, these IMs have also been explored as membrane exchange humidifier for fuel cells [34,35] or energy recovery ventilators for building [36]. Our recent work on water vapor removal from natural gas also confirms that the removal of paper layer in the thin film composite membranes significantly increases water vapor permeances without influencing the water/methane selectivity [18,37].

The objective of this study is to investigate the impregnated membranes containing mechanically strong porous support filled with hydrophilic polymers for water purification using forward osmosis. First, a series of IMs are prepared and characterized for water permeability and salt rejection. Second, the IMs are tested in the laboratory under the FO mode to understand the effect of operating parameters (including the salt content in the draw solution, and the flow rates of the feed and draw solution) on separation performance. Finally, the separation performance of the FO membranes is compared with commercial ones or others reported in the literature, and the potential of IMs is evaluated. The effect of concentration polarization on the water flux in these IMs will also be discussed.

CHAPTER 2: THEORY

2.1. THEORY OF WATER TRANSPORT IN MEMBRANES

Water flux, J_W (litter/m^2 hour or LMH), through a dense polymer film follows the solution-diffusion mechanism and can be described by [38-40]:

$$J_W = A_W(\Delta P - \Delta\pi) = \frac{P_W}{l}\frac{\bar{V}_W}{R_g T}[(p_F - p_P) - (\pi_F - \pi_P)] \quad (1)$$

where A_W is the water permeance (LMH/bar), Δp is the pressure difference across the membrane (bar), and $\Delta\pi$ is the osmotic pressure difference (bar) across the membrane. P_W (cm^2/s) is water permeability, l (cm) is the film thickness at equilibrium with the feed water, $\bar{V}_W$ is the molar volume of water (18 cm^3/mol), R_g is the gas constant (83.1 cm^3 bar/mol K) and T is the temperature (K). The subscript of F and P indicates the property on the membrane feed side and permeate side, respectively.

For pure water permeation, there is no osmotic pressure difference across the membrane (*i.e.*, $\pi_F = \pi_P$), and thus the water flux is given by:

$$J_W = A_W(p_F - p_P) = \frac{P_W}{l}\frac{\bar{V}_W}{R_g T}(p_F - p_P) \quad (2)$$

During the FO operation, there is no pressure difference across the membrane (*i.e.*, $p_F = p_P$), and thus the water flux is given by [17]:

$$J_W = A_W(\pi_F - \pi_P) = \frac{P_W}{l}\frac{\bar{V}_W}{R_g T}(\pi_F - \pi_P) \quad (3)$$

where π_D, instead of π_P, is used to characterize the permeate osmotic pressure, since the permeate stream is often called the draw solution during the FO operation.

The salt flux, J_S (g/m^2 hour or gMH), is often expressed by [38,39]:

$$J_S = B\left(C_{S,F} - C_{S,P}\right) = \frac{P_S}{l}\left(C_{S,F} - C_{S,P}\right) \tag{4}$$

where B (cm/s) is the salt permeance in the membrane, P_S (cm^2/s) is the salt permeability, and $C_{S,P}$ and $C_{S,F}$ is the salt concentration (g/cm^3) in the permeate and feed solutions, respectively.

According to the solution-diffusion model, the salt permeability can be expressed [38]:

$$P_S = D_S \times K_S \tag{5}$$

where D_S is the average salt diffusivity (cm^2/s) in the polymer and K_S [(g salt/cm^3 swollen polymer) / (g salt/cm^3 solution)] is the salt solubility in the polymer. The salt solubility is given by [40]:

$$K_S = \frac{C_{S,F}^m}{C_{S,F}} \tag{6}$$

where $C_{S,F}^m$ (g salt/cm^3 swollen polymer) is the equilibrium salt concentration in the membrane surface in contact with the feed solution.

The osmotic pressure (π) is often related to the total ion concentration. In this study, NaCl solutions are used, and the osmotic pressure can be estimated using the van't Hoff equation [41,42]:

$$\pi = 2C_S R_g T / M_{W,S} \tag{7}$$

where $M_{W,S}$ is the molecular weight of the salt. The efficiency of salt separation by membranes is described using the salt rejection, R_S [38,39]:

$$R_S \equiv \left(1 - \frac{C_{S,P}}{C_{S,F}}\right) \times 100\% \tag{8}$$

2.2. CONCENTRATION POLARIZATION

The adverse effect of concentration polarization on the membrane applications has been well documented, such as ultrafiltration [19,43], pervaporation [44], gas and vapor separation [18,45] and FO [15,16,20]. Fig. 2 presents the concentration polarization phenomena for FO application in two membranes including a conventional asymmetric membrane and a symmetric membrane (impregnated membrane).

(a) Conventional FO membranes (b) Impregnated membranes

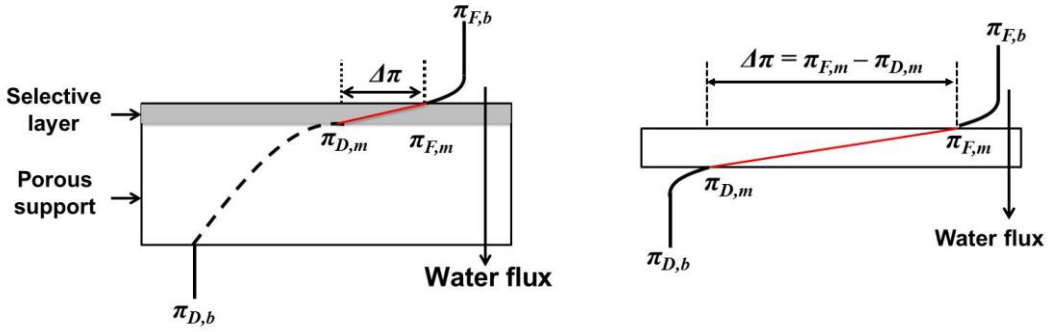

Fig. 2. Effect of concentration polarization on the driving force for water permeation based on the osmotic pressures in (a) a conventional asymmetric FO membranes with the selective layer facing the feed solution, and (b) an impregnated membrane under FO mode.

Fig. 2a exhibits the concentration polarization in a typical FO membrane, which is comprised of a thin dense selective layer on the top of porous support layer. The selective layer is faced with the feed solution, and the porous support is faced with the draw solution. As the water selectively diffuses through the selective layer, the solute content on the feed solution adjacent to the membrane increases (*i.e.*, external concentration polarization), while the salt content on the draw side adjacent to the membrane in the porous support is diluted (*i.e.*, internal concentration polarization) [12].

Fig. 2b shows water diffusion in a dense symmetric membrane. The membrane does not have a porous support and therefore, there is no internal concentration polarization. Considering

external concentration polarization on both sides of the membrane, the following equation has been derived [42,46].

$$J_W = A_W \frac{\pi_{D,b} \exp(-J_W/k_F) - \pi_{F,b} \exp(J_W/k_D)}{1 + B/J_W \left[\exp(J_W/k_D) - \exp(-J_W/k_F)\right]} \quad (9)$$

where $\pi_{D,b}$ and $\pi_{F,b}$ are the osmotic pressure (bar) of the bulk draw solution and feed solution, respectively. k_D (cm/s) and k_F (cm/s) are the mass transfer coefficient in the draw solution and feed solution adjacent to the membrane, respectively.

Current symmetric membranes require large thickness to obtain good mechanical property and therefore, they have not been extensively investigated for FO applications [15]. Nevertheless, the internal concentration polarization is regarded as one of the significant obstacles to the implementation of the FO processes for practical applications [7]. The goal of this study is to explore the use of thin symmetric membranes for FO applications by preparing impregnated membranes (as shown in Fig. 1b) providing good mechanical properties and high water flux.

CHAPTER 3: EXPERIMENTAL SECTION

3.1. MATERIALS

Poly(ethylene glycol) diacrylate (PEGDA, Mn=700 g/mol) and 1-hydroxylcyclohexyl phenyl ketone (HCPK) were purchased from Sigma-Aldrich Chemical Co. (Milwaukee, WI) and used as received. Ethanol as the solvent was purchased from Fisher Scientific Co. (Waltham, MA, US). The porous support of Solupor® (with a pore size of 0.8 μm, a porosity of 84% and a thickness of 45 μm) was purchased from Lydall Performance Materials, Inc. (Rochester, NH). The HTI OsMem™ TFC-ES membrane was purchased from Hydration Technology Innovations (Albany, OR). The reverse osmosis membrane of Filmtec™ SW30XLE was purchased from Dow Water & Process Solutions (Minneapolis, MN). Deionized water was produced using a Milli-Q water purification system (EMD Millipore, Billerica, MA).

3.2. PREPARATION OF FREE-STANDING POLYMER FILMS

Free-standing polymer films were prepared using PEGDA via free-radical UV-photopolymerization [47,48]. First, a solution containing PEGDA, solvent (deionized water or ethanol) and HCPK was prepared and stirred for 5 hours. The HCPK content is 0.1 wt.% of the PEGDA, and the solvent content was varied from 0 to 80 wt.%. Secondly, the solution was sandwiched between a quartz plate and a glass plate separated by spacers with known thickness and exposed to UV-light with a wavelength of 254 nm in a Ultraviolet Crosslinker (CX-2000, Ultra-Violet Products Ltd, Upland, CA) for 120 s at 3.0 mW/cm^2. The thickness of the polymer film was controlled by the thickness of the spacers. Finally, the film was removed from the plate and soaked in deionized water for 24 hours, before drying in air for 24 hours and then in a

vacuum oven for overnight. Fig. 3 shows the chemical structure of PEGDA and schematic of crosslinked PEGDA (XLPEGDA) [47].

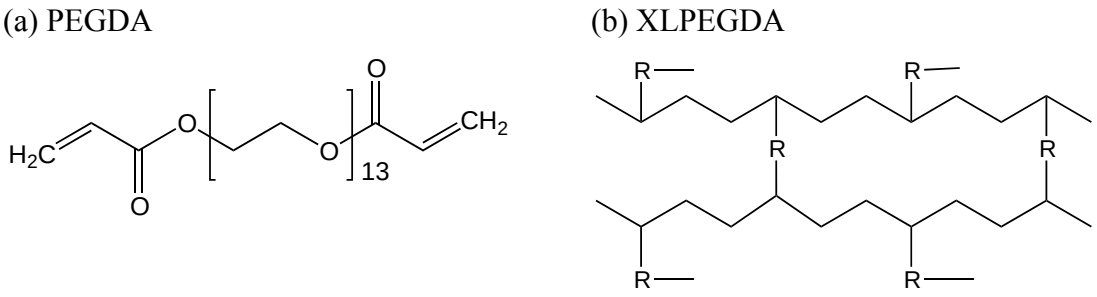

Fig. 3. (a) Structure of poly(ethylene glycol) diacrylate (PEGDA). (b) Schematic of a crosslinked PEGDA (XLPEGDA). R is $COO(CH_2CH_2O)_{13}OCO$ from the PEGDA.

3.3. PREPARATION OF IMPREGNATED MEMBRANES

To prepare impregnated membranes, the first step is to prepare prepolymer solutions containing PEGDA and HCPK (0.1 wt.%). Ethanol was used as the solvent since the Solupor support is hydrophobic and ethanol can easily wet the support. Second, a sheet of Solupor support was taped onto a Teflon plate. The solution was coated using a foam brush for two times on each side of the Solupor support. Third, after removing the liquid on the support surface using paper, the support was sandwiched between plates and exposed to the UV light for 72 s for the PEGDA to polymerize. Finally, the impregnated membrane was soaked in deionized water, and the water was changed twice to remove the ethanol from the membrane.

3.4. CHARACTERIZATION OF POLYMER PHYSICAL PROPERTIES

The conversion of the acrylate groups in the PEGDA is monitored using attenuated total reflection Fourier-transform infrared (ATR-FTIR) spectroscopy (Vertex 70, Billerica, MA). The resolution of the measurement was 4 cm^{-1}.

The sol and gel fraction in the prepared free standing films and IMs was determined [47]. After the polymerization, the polymer sample was dried and weighted (with a mass of m_0). The sample was then immersed in the deionized water for 24 hours to remove the sol, before being dried and weighted again (with a mass of m_{gel}). The gel fraction (w_{gel}) can be calculated:

$$w_{gel} = \frac{m_{gel}}{m_0} \times 100\% \tag{10}$$

The film thickness was measured using a digital micrometer (Starrett 2900, The L.S. Starrett Co., MA). The films have a thickness ranging from 30 μm to 500 μm.

The sample density at the room temperature was determined using a balance equipped with a density kit (XS 64, Mettler-Toledo Inc., Columbus, OH). Iso-octane was used as an auxiliary liquid. The following equation is used to obtain the density of the polymer samples (ρ_p) [47]:

$$\rho_p = \frac{m_{air}}{m_{air} - m_{liquid}} \left(\rho_{liquid} - \rho_{air} \right) + \rho_{air} \tag{11}$$

where m_{air} and m_{liquid} is the weight of the sample in air and iso-octane, respectively, and ρ_{air} and ρ_{liquid} is the density of air and iso-octane, respectively.

The hydrophilicity of the polymer surface was determined using a contact angle goniometer (Rame-hart Model 190, Rame-hart Instrument, Succasunna, NJ, US). Deionized water was used as the probing liquid.

3.5. CHARACTERIZATION OF WATER TRANSPORT PROPERTIES

The water absorption in the polymer samples was measured at the room temperature (22°C). After immersing in the deionized water to remove the sol, the sample was dried and weighted with a mass of m_{dry}. The sample was then immersed in the deionized water for 24 hours to reach equilibrium. The weight of the wet sample was measured to be m_{wet}. The percent of water

absorption (w_W) was calculated as below:

$$w_W = \frac{m_{wet} - m_{dry}}{m_{wet}} \times 100\% \tag{12}$$

The solvent absorbed in the polymer often has the density the same as the liquid. Assuming the additive mixing of the polymer and water, the volume fraction of water in the hydrated polymer sample, v_W, can be calculated as follows [47]:

$$v_W = \frac{(m_{wet} - m_{dry}) / \rho_W}{(m_{wet} - m_{dry}) / \rho_W + m_{dry} / \rho_p} \tag{13}$$

where ρ_W is the water density (g/cm^3).

The water permeability in the free standing films and IMs was determined using a dead-end filtration system [49,50]. The permeation cell (Model UHP-43, Advantec MFS, Inc, Dublin, CA) has a magnetic stir bar which can be tuned for operation at 300 – 1200 rpm. After the membrane sample was mounted, the cell was filled with the solution and pressurized with pure-gas nitrogen. The permeated water is collected using a beaker and the weight was monitored with time. Before the measurement, the film was equilibrated with water at 20 psig for overnight. The water hydraulic permeance and permeability across the membranes can be calculated using Eq. 1.

3.6. CHARACTERIZATION OF SALT TRANSPORT PROPERTIES

The salt permeability in the membranes was directly determined using the dead-end filtration system. The feed solution contained 2.0 g/L NaCl. The salt concentration in the feed and permeate was monitored by measuring conductivity with a conductivity meter (Oakton CON 11 meter, Oakton Instruments, Vernon Hills, IL). Equations 3 and 4 can be used to calculate the

water and salt permeance, respectively. To ensure that the salt content in the feed solution did not change significantly during the data recording, the feed solution was changed frequently, and the accumulated water permeate was less than 5% of the feed solution during the data recording.

The salt diffusivity and solubility was also determined using kinetic desorption experiment [51]. The impregnated membrane was first equilibrated with deionized water, and then cut to a disk shape with a diameter of 1 inch. Second, the sample was soaked in 15 ml of 0.5 M NaCl solution (or 29.2 g/L) for 48 hours at room temperature (~23°C) for the sample to equilibrate with the NaCl solution. Third, after the sample was taken out the solution and removed off the liquid on the surface, it was immersed in the deionized water (referred as extraction solution). The salt content in the extraction solution was monitored as a function of time using the conductivity meter. The solution was continuously stirred to ensure that the extraction solution was well-mixed. The NaCl diffusivity in the polymer sample, D_S, can be estimated using the Fickian diffusion model [52-54]:

$$D_S = 0.196 \cdot l^2 \left[\frac{d\left(M_t / M_\infty\right)}{d\left(t^{1/2}\right)} \right]^2 \tag{14}$$

where M_t (g) is the mass of NaCl in the extraction solution at time t, and M_∞ (g) is the mass of NaCl in the extraction solution at equilibrium. Eq. 14 is only valid when the value of M_t / M_∞ is less than 0.6.

The NaCl solubility, K_S, is calculated as the ratio of the concentration of NaCl in the polymer at equilibrium to that of the salt solution (29.2 g/L NaCl in this study). The NaCl sorbed in the membrane is assumed to the same as the total salt in the extraction solution at equilibrium (*i.e.*, M_∞) [50,51].

3.7. CHARACTERIZATION OF MEMBRANE PERFORMANCE UNDER FO MODE

The IMs were evaluated for FO applications using a custom-built system similar to those reported in the literature [15]. The permeation cell (SEPA CF II, GE Water & Process Technologies) was modified to have the countercurrent flow for the feed and draw solution. The permeate carriers or spacers with a thickness of 272 μm (part number 1142817, GE Infrastructure Water & Process Technologies, Minnetonka, MN) were used for both the feed and draw solution sides to provide mechanical support and flow channels [18]. The effective membrane area is 140 cm^2. Two peristaltic pumps (model 913, MityFlex, Anko Products, Inc., Bradenton, FL) were used to circulate the solutions into the permeation cell.

In the FO operation, the feed solution is deionized water and the draw solution is salty water containing various amount of NaCl. The draw solution container is large enough to retain approximately same draw solution concentration during the experiment [55]. In typical operation, the flow superficial velocity in the spacer channels (v_∞) was kept at 38 cm/s and the Reynolds number (R_e) was 210 ($R_e = 2Hv_\infty/\nu$, where H is the height of the flow channel or permeate spacer, and ν is the solution kinetic viscosity) [56]. The weight change of the draw solution was monitored as a function of time to determine the water flux using Eq. 3. The salt flux (J_S) can be determined by monitoring the change of the salt concentration in the feed solution as function of time, and the salt permeance can be calculated using Eq. 4 [22].

CHAPTER 4: RESULTS AND DISCUSSION

4.1. Preparation and characterization of impregnated membranes (IMs)

To prepare impregnated membranes, the prepolymer solution needs to be compatible with the Solupor support so that it can easily penetrate into the pores. Since Solupor is made of hydrophobic polyethylene, the ethanol, instead of water, is used as the solvent for PEGDA in the prepolymer solution. Fig. 4 compares the appearing of the Solupor support and the prepared impregnated membrane. As shown in Fig. 4(b), the logo at the bottom is not clear since the support itself is opaque due to the porous structure. On the other hand, the impregnated membrane is transparent (cf. Fig. 4c), presumably because the polymer completely fills up the pores, resulting in the film with relatively constant refractive index and thus transparency.

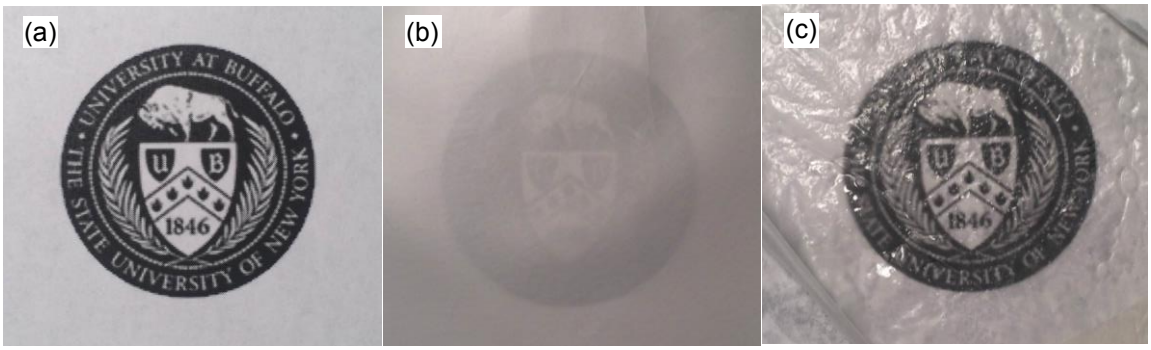

Fig. 4. Photographs of (a) logo only, (b) a Solupor support on the top of the logo, and (c) an impregnated membrane on the top of the logo.

The ATR-FTIR was used to characterize the conversion of acrylate groups of the monomer, PEGDA. Fig. 5 compares a typical spectrum of a polymer and an impregnated membrane prepared from 80% PEGDA and 20% ethanol (XLPEGDA80) with that of monomer PEGDA. The acrylate groups have characteristic peaks of 810, 1190, and 1410 cm^{-1}, which practically

disappear in the spectra of the polymer and impregnated membrane, indicating the almost complete conversion of PEGDA [47]. The IR spectra for other XLPEGDA polymers and impregnated membranes are similar to that of XLPEGDA80 and they are not shown here. The results are not surprising since the PEGDA has been shown to be easily photo-polymerized with complete conversion [47,49,53]. The spectrum of the Solupor support is also shown in Fig. 5, which has no interference with the characteristic peaks of the acrylate groups.

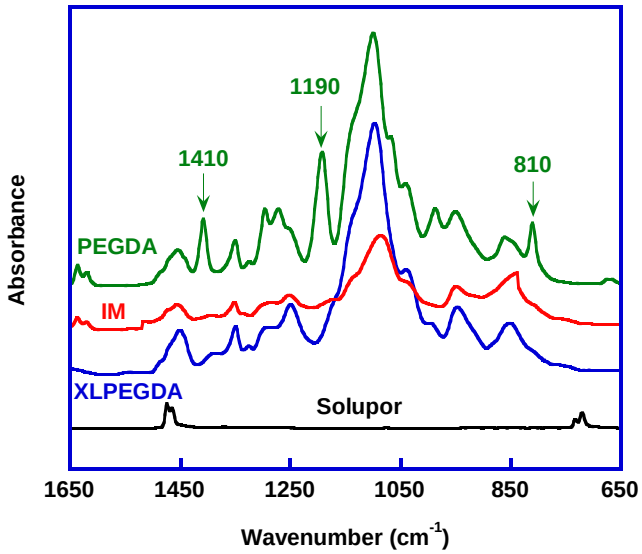

Fig. 5. Comparison of a typical ATR-FTIR spectrum of a polymer film and an impregnated membrane (IM) prepared from 80% PEGDA and 20% ethanol (XLPEGDA80) with that of liquid PEGDA and the Solupor support.

Table 1 shows physical properties of the impregnated membranes. The membranes have the gel fraction of near one, confirming the almost completion of acrylate conversion. The gel fraction is also independent of the composition of the prepolymer solutions, indicating the negligible effect of the ethanol content on the polymerization conversion. These results are consistent with the earlier work on the free standing films from PEGDA and H_2O [47,52,53].

Table 1
Physical properties of impregnated membranes prepared from PEGDA and ethanol (EtOH).

Prepolymer composition PEGDA:EtOH	Gel fraction (%)	Impregnated membrane density (g/cm^3)	Water sorption w_w (%)	Contact angle*
100:0	99	1.145±0.005	32.1	47.0±0.1
80:20	99	1.151±0.005	39.7	42.1±0.1
60:40	99	1.159±0.005	55.7	41.1±0.2
40:60	99	1.152±0.005	72.4	N/A
20:80	97	1.154±0.005	N/A	N/A

* for the free standing films.

Table 1 also shows the density of IMs prepared from PEGDA and ethanol. The density values are independent of prepolymer solutions. The Solupor support has a density of 0.156 g/cm^3 and a porosity of 0.84. Assuming that the pores are completely filled by the XLPEGDA (with a density of 1.182 g/cm^3), the density of IMs is 1.149 g/cm^3, which is very similar to those measured, as shown in Table 1.

The contact angle results for the free standing films are presented in Table 1. The XLPEGDAs are more hydrophilic than the Solupor support with a contact angle of 92.2 ± 0.1 using water as a probing liquid.

4.2. PURE WATER SORPTION AND PERMEATION IN IMPREGNATED MEMBRANES

Fig. 6 compares the water sorption behavior of the IMs prepared from PEGDA/EtOH with that of free standing polymer films prepared from PEGDA/EtOH and PEGDA/H_2O. Increasing the solvent (water or ethanol) content in the prepolymer solutions increases water sorption in all samples, which can be ascribed to the lower crosslinking density with lower monomer concentration [47]. Fig. 6 shows that the use of ethanol as the solvent yields the polymer with

higher water uptake, compared to that from the prepolymer solution containing water. The impregnated membranes show water uptake similar to the corresponding free standing polymer samples, indicating that the Solupor support has minimal effect on the water sorption in the polymers.

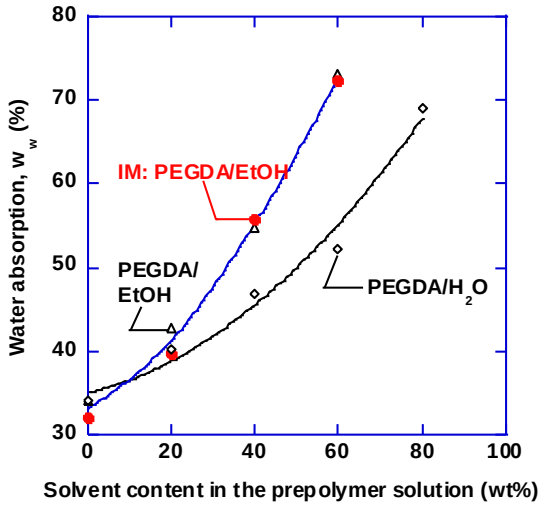

Fig. 6. Comparison of water sorption of the impregnated membranes (IMs) prepared from PEGDA/EtOH with that of the free standing polymer films prepared from PEGDA/EtOH and PEGDA/H_2O [47].

Fig. 7(a) exhibits the effect of feed pressure on pure water permeability in the free standing films prepared from the mixtures of PEGDA and EtOH. All the free standing samples have a thickness of around 250 μm. The pure water permeability is independent of feed pressure. Increasing the solvent content in the prepolymer solution can significantly increase water permeability, particularly as the EtOH content increases above 40%. For example, as the EtOH content in the prepolymer solutions increases from 40% to 60%, pure water permeability in the resulting polymers increases from 2.3×10^{-4} cm^2/s to 0.026 cm^2/s by two orders of magnitude. This increase is consistent to the morphology change of XLPEGDA40, which became opaque

after polymerization, indicating it underwent a polymerization induced phase separation process. The more open structure leads to higher water diffusion and permeability, compared to the polymers polymerized without the phase change [52].

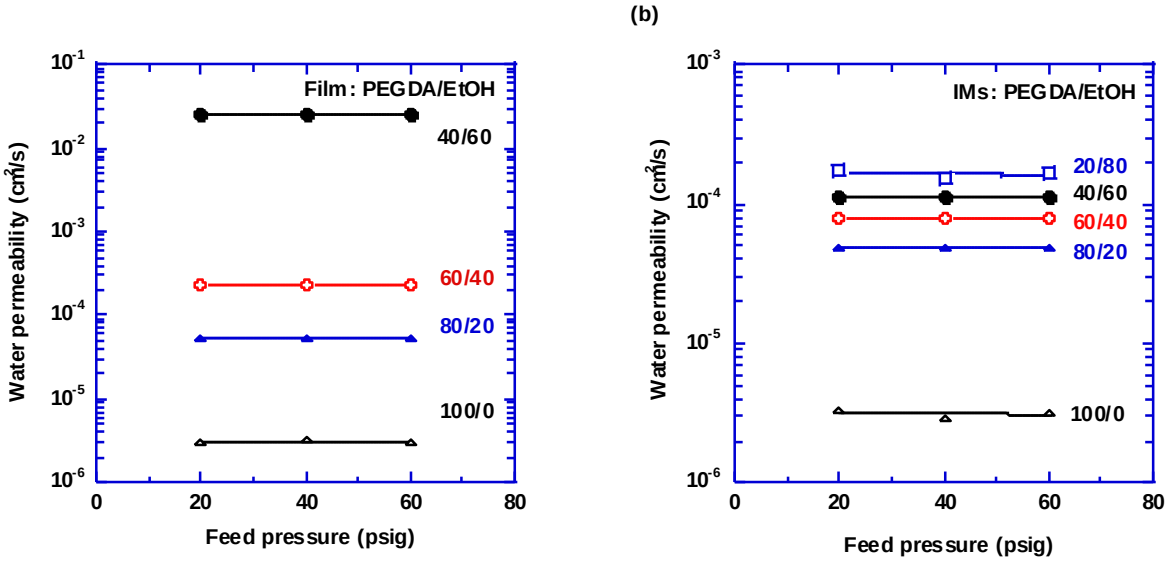

Fig. 7. Effect of the feed pressure and prepolymer composition on pure water permeability in (a) free standing polymer films and (b) impregnated membranes. 10^{-6} cm^2/s = 0.263 L μm/(m^2 hour bar).

Fig. 7(b) shows the water permeability in a series of impregnated membranes prepared from the mixtures of PEGDA and EtOH. These membranes have a thickness between 43 μm to 55 μm after swelling in the deionized water overnight, which is consistent to the Solupor thickness of about 45 μm. The impregnated membranes show similar behavior to the free standing films, *i.e.*, the water permeability is independent of feed pressure, and it increases with increasing EtOH content in the prepolymer solutions. On the other hand, no phase separation was observed for the impregnated membranes, even as the EtOH content increases to 80% in the prepolymer solution.

Fig. 8 compares the pure water permeability in the IMs with that in the free standing films.

At the EtOH content of less than 20%, these two samples show very similar water permeability. At the EtOH content of higher than 20%, the free standing films start to show much higher permeability than the IMs. It seems that the hydrophobic Solupor support restricts the swelling of the hydrophilic XLPEGDA, avoiding the phase separation during the polymerization. On the other hand, the free standing films have the strong degree of swelling and phase separation during the polymerization, leading to extraordinarily high water flux [52].

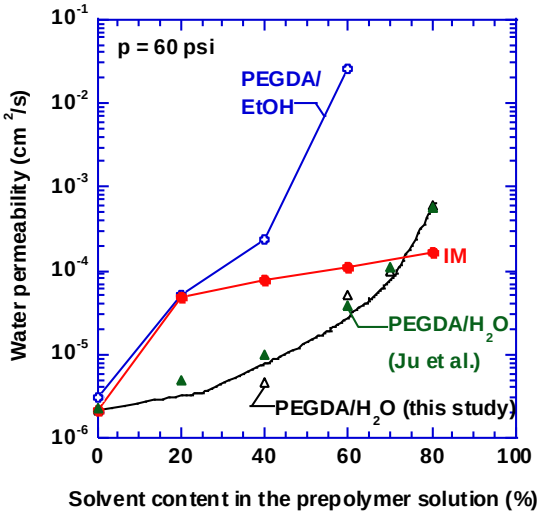

Fig. 8. Comparison of water permeability of impregnated membranes (IMs) prepared from PEGDA/EtOH with that of the free standing polymer films prepared from PEGDA/EtOH and PEGDA/H_2O [52] at a feed pressure of 60 psig and 23°C. The curves are to guide the eye.

Fig. 8 also compares water permeability in the free standing films prepared from PEGDA/EtOH and those from PEGDA/H_2O. Similar to the behavior of water sorption, polymers from PEGDA/EtOH show higher permeability than those from PEGDA/H_2O [52].

4.3. SALT REJECTION DETERMINED USING A DEAD-END FILTRATION SYSTEM

The salt rejection of the IMs was first investigated using a dead-end filtration system and a

salt solution containing 2.0 g/L (or 0.034 M) NaCl at feed pressures of 20, 40 and 60 psig. To understand the effect of concentration polarization on the top surface of membranes, the stirring rate was varied at 300, 600 and 900 rpm, and the water permeability and salt rejection are calculated and shown in Fig. 9.

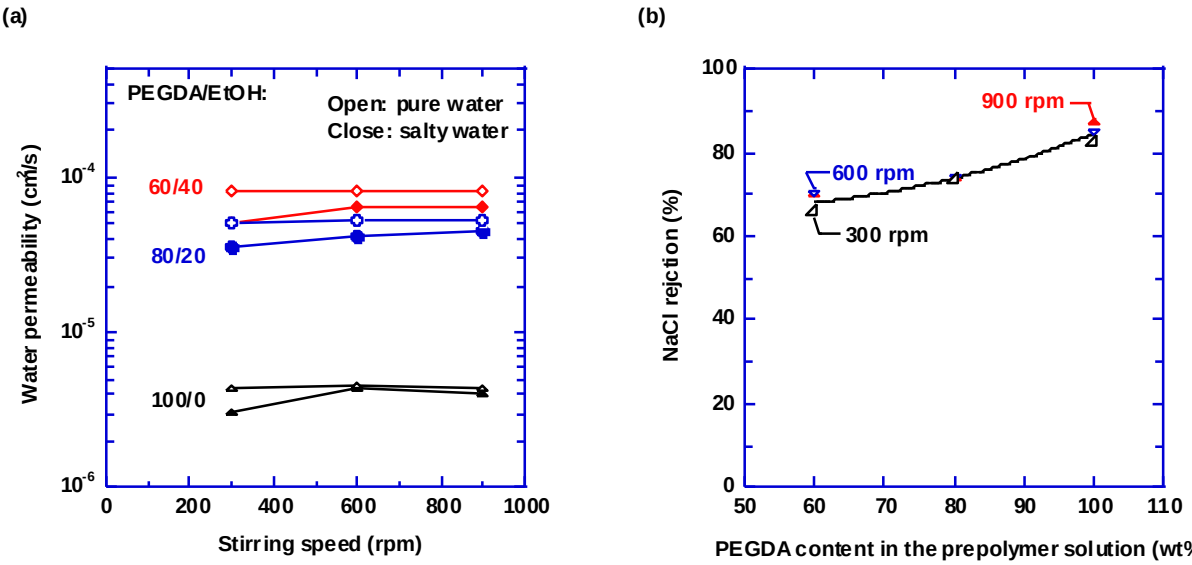

Fig. 9. (a) Comparison of pure water permeability and salty water permeability of impregnated membranes (IMs) prepared from PEGDA/EtOH in a dead-end filtration system with a stirring rate of 900 rpm. (b) Effect of prepolymer solution composition on the NaCl rejection rate, R_S, calculated using Eq. 8. The salty solution contains 2.0 g/L NaCl at 60 psi.

As shown from Fig. 9(a), increasing the EtOH content in the prepolymer solution increases the water permeability, which is consistent to the pure water permeability. On the other hand, the salty water permeability is slightly lower than the pure water permeability, which may be ascribed to the following two reasons. First, the salty water may dewater the crosslinked PEGDA, leading to the lower water update and thus permeability [57]. Second, there exists concentration polarization on the membrane surface adjacent to the feed solution. As the water selectively permeates through the membrane, the NaCl content builds up adjacent to the membrane surface, increasing the apparent osmotic pressure on the membrane surface and

decreasing the water flux [57]. The effect of concentration polarization on permeation is also illustrated in Fig. 9b. Increasing the stirring rate from 300 rpm to 900 rpm slightly increases the salt rejection rate, R_S, calculated using Eq. 8. However, higher stirring rate than 900 rpm may be needed to further reduce the concentration polarization.

Fig. 9b also shows that lower EtOH content in the prepolymer solutions results in the IMs with higher salt rejection. In general, lower solvent content leads to lower water sorption and tighter polymer networks [47,50], both contributing to stronger size sieving ability and thus higher salt rejection rate.

4.4. SALT PERMEATION PROPERTIES CHARACTERIZED USING KINETIC SORPTION EXPERIMENTS

The salt permeation properties in the IMs can also be determined by kinetic sorption experiments [50,51]. Eq. 14 is used to calculate the salt diffusivity at the early stage of salt desorption, where M_t/M_∞ is less than 0.6 [54,58-60]. Fig. 10 presents the NaCl diffusivity and solubility as a function of water volume fraction in the in the IMs at equilibrium. The salt diffusivity increases exponentially with the increase in the reciprocal free volume [40,61], while the free volume is proportional to the water volume fraction in the membranes [50,54,58,62]. On the other hand, the IMs consisting of XLPEGDA40 does not follow this trend, since the membrane undergoes polymer induced phase separation during the polymerization [49,63,64]. The water phase may not be interconnected, and thus, it does not contribute to the diffusivity as effective as expected for the water in the homogenous phase. Generally, the water phase may not be considered as the free volume.

Fig. 10a also compares the salt diffusivity in IMs with that in the free standing films prepared

from PEGDA and water [50]. Both series of polymers show the same trend, and the diffusivity is lower than expected based on the water volume fraction when the polymers have phase separation. The NaCl diffusivity in these hydrogels approaches that in the pure water (*i.e.*, v_W=1) [65], as the free volume increases.

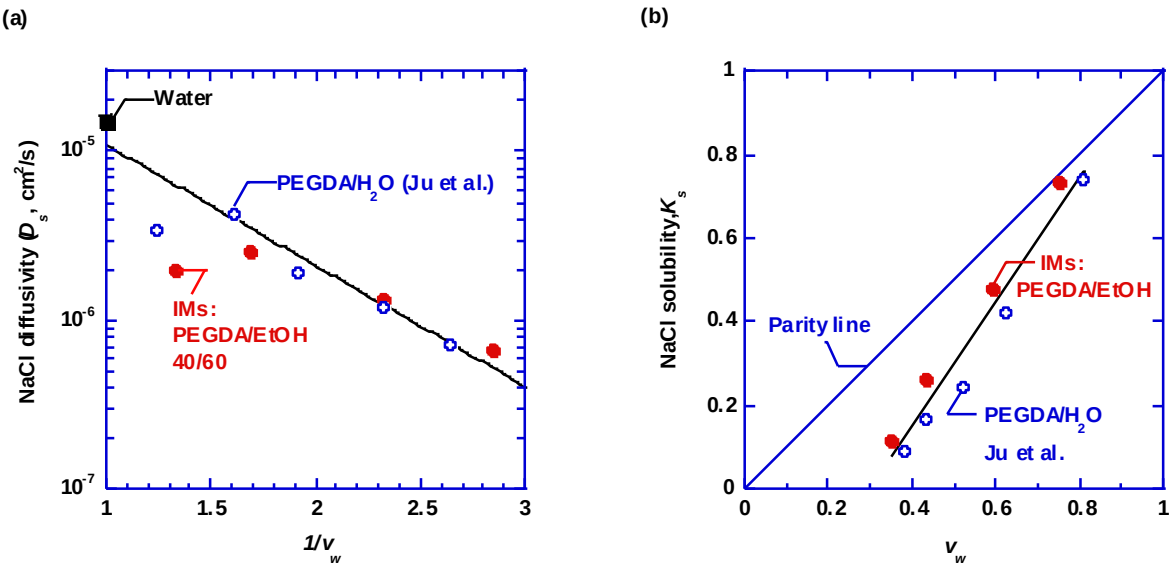

Fig. 10. Effect of water volume fraction (v_w) in the impregnated membranes at equilibrium on (a) NaCl diffusivity and (b) NaCl solubility at room temperature. The results are also compared with those in the free standing films prepared from PEGDA and H_2O reported by Ju et al. [50].

Fig. 10b shows the correlation between NaCl solubility and water volume fraction in the IMs. The NaCl solubility increases with increasing equilibrium water content of the membranes. Fig. 10b also shows a parity line, indicating the equal salt sorption in the water present in the membranes and pure water. The amount of NaCl sorption in the swollen polymers is lower than that in the pure water, and the difference becomes more significant for the polymers with lower water sorption (v_w). This phenomenon is presumably ascribed by the effect of polymers on the salt sorption in the water. The polymer network itself has negligible salt sorption [54], and the presence of polymer chains in the water apparently decreases salt sorption. The correlation

between the NaCl sorption and water volume fraction in the IMs is also similar to that in the free standing polymer films prepared from PEGDA and water [50].

The NaCl permeability is calculated from the solubility and diffusivity, and the results are shown in Fig. 11. NaCl permeability decreases exponentially with the reciprocal water volume fraction (*i.e.*, $1/v_w$) or the reciprocal free volume, which is consistent to the salt diffusion behavior. This behavior has been theoretically modeled by Yasuda and coworkers [54,62]. The dependence of the NaCl permeability on water volume fraction is also similar to that of free standing films prepared from PEGDA/H_2O [50].

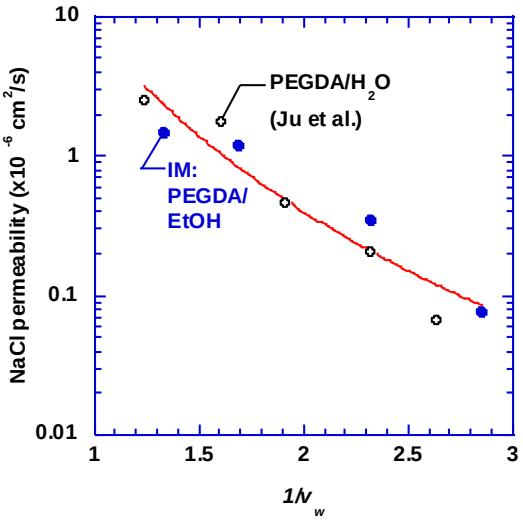

Fig. 11. NaCl permeability in impregnated membranes (IMs) as a function of $1/v_w$., which is also compared with that in the free standing films prepared from PEGDA and H_2O reported by Ju et al. [50].

4.5. IMPREGNATED MEMBRANES FOR FO APPLICATIONS

Before testing the IMs for FO applications, commercial membranes including HTI OsMem^{TM} TFC-ES (abbreviated as HTI) and Dow Filmtec SW30-XLE (abbreviated as SW30-XLE) were tested to establish the baseline, since these two membranes have been widely evaluated for FO

applications [20,66]. Table 2 records the water permeances for the HTI, SW30-XLE and IMs operating under the FO mode. The feed solution is pure water and the draw solution is 1.0 M NaCl solution with an osmotic pressure of 49.2 bar. The superficial velocity in the feed and draw flow channel is 38 cm/s, and the Reynolds number is 210. The HTI membrane shows a water flux of 11 LMH, salt flux of 7.0 gMH, and salt rejection of 98.9%, which are comparable to the literature value of 14 LMH, 5.0 gMH and 99.4%, respectively [67]. The discrepancy may be ascribed to the difference in the testing conditions. In this study, the permeation cell was operated with a Re number of 210 with a permeate carrier. However, in the literature, the permeation cell was operated with a Re number of 1125 without the spacers [67]. Both factors may contribute to higher water flux, compared to those obtained in this study.

Table 2
Water and salt permeances in the membranes for FO applications, compared with those from the dead-end filtration system. The FO was operated with a feed solution of Milli-Q water and a draw solution of 1.0 M NaCl solution at room temperature. The Reynolds number in both channels was 210.

Membranes	Pure water permeance (LMH/bar)	FO operation			
		Water permeance (LMH/bar)	Performance ratio	Salt permeance (gMH)	Salt rejection (%)
HTI	1.5±0.1	0.23±0.01	0.15±0.01	5.9	98.9
SW30-XLE	1.4±0.1	0.046±0.005	0.032±0.003	1.3	99.0
IM-XLPEGDA80	0.28±0.02	0.052±0.005	0.18±0.02	7.0	95.3
IM-XLPEGDA60	0.40±0.03	0.077±0.005	0.19±0.02	7.1	96.8
IM-XLPEGDA40	0.59±0.03	0.10±0.01	0.17±0.02	100	65.5

As shown in Table 2, increasing the EtOH content in the prepolymer solution for the IMs increases the FO water permeance, which is consistent to the pure water permeation results from the dead-end cell systems. The water permeances under the FO mode are compared with the pure and salty water permeances from the dead-end filtration system. The performance ratio is

defined as the water permeance ratio of the FO to the dead-end filtration system [12,15]. The ratio is also equal to the percentage of driving force effectively inducing the water transport across the membrane during the FO [12]. The SW30-XLE membranes have been shown to have low values of performance ratio, due to the internal and external concentration polarization. The IMs have higher values of the performance ratio (about 0.18), compared with the SW30-XLE membrane (with the performance ratio value as low as 0.032). The result also indicates that by eliminating the open porous structure in the FO membranes, the internal concentration polarization can be significantly reduced.

The performance ratio of 0.18 in IMs indicates that there exists significant external concentration polarization for the IMs. This may partially explain that the performance ratio of IMs is only slightly higher than that in HTI membranes. It should also be pointed out that the water permeances in these IMs are still lower than that of HTI membranes.

The reverse salt flux (gMH) of the IMs in IM-XLPEGDA80 and XLPEGDA60 is 7 gMH, which is comparable to that of HTI membranes and much higher than that in SW30-XLE. Increasing the EtOH content in the prepolymer solution seems to have negligible effect on salt flux for the IMs of XLPEGDA80 and XLPEGDA60. On the other hand, the IM consisting of XLPEGDA40 has the salt flux of 100 gMH, indicating the much more open structure compared with the other IMs.

Table 3 summarizes the NaCl permeability (P_S) calculated from the three different experiments, including the hydraulic dead-end permeation, kinetic salt desorption, and forward osmosis. The salt permeance decreases with decreasing the EtOH content in the prepolymer solution, which is consistent with the results in Fig. 7(b). The salt permeability values follow the order from high to low: kinetic desorption > dead-end filtration > FO. In general, there is the

least effect of concentration polarization in the kinetic desorption experiments, due to the intensive stirring. The dead-end filtration system has stirring on the feed side. The forward osmosis seems to suffer the most from the concentration polarization.

Table 3
Comparison of the NaCl permeability (cm^2/s) in the IMs from three experiments, hydraulic dead-end permeation with a NaCl content of 0.034 M, kinetic salt desorption with a NaCl solution of 0.5 M and forward osmosis with a draw solution of 1.0 M NaCl and a feed solution of pure water.

Testing condition and membranes	NaCl permeability (cm^2/s)		
	Dead-end filtration	Kinetic desorption	Forward osmosis
IM: XLPEGDA100	1.2×10^{-9}	7.7×10^{-8}	
IM: XLPEGDA80	3.4×10^{-8}	3.5×10^{-7}	1.7×10^{-8}
IM: XLPEGDA60	6.0×10^{-8}	1.2×10^{-6}	1.8×10^{-8}
IM: XLPEGDA40		1.5×10^{-6}	2.9×10^{-7}

The external concentration polarization for the IMs can be investigated by varying the flow rate and the Reynolds number in the permeation cell. The typical operating condition has the Reynolds number of 210 for the feed and draw solution flow channel (10 cm^3/s or 38 cm/s). The flow rate was also increased to 90% of the maximal flow rate provided by the pump with a flow velocity of 68 cm/s and Reynolds number of 380. Table 4 summarizes the water permeances at various flow rates in various membranes. The flow rate shows negligible effect on the water permeance within the flow rate investigated. The membranes also show similar NaCl flux at various flow rates. The Reynolds number investigated here is still much lower than that (1125) used in most of studies reported. There is a need to study the effect of external concentration polarization at higher flow rates, which, however, cannot be achieved using the current apparatus.

Table 4
Water permeance (A_W, LMH/bar) for various membranes and flow rates of the feed and draw solution. FO testing condition: 1 M NaCl solution as the draw solution; pure water as the feed solution; T= 23 °C.

Feed solution Re	Draw solution Re	HTI TFC-ES	Filmtec SW30-XLE	IM: XLPLEDA80	IM: XLPEGDA60
210	210	0.221	0.0464	0.0519	0.0771
210	380	0.218	0.0469	0.0510	0.0763
380	210	0.229	0.0527	0.0521	0.0783

Fig. 12 shows the effect of the NaCl concentration of the draw solution on the salt permeability in various IMs. The feed solution is pure water. In general, increasing the salt concentration of the draw solution increases the salt rejection rate, which can be explained below. As the NaCl content increases in the draw solution, the driving force for water permeation increases, leading to the increase in the water flux and more significant dilutive effect on the membrane surface on the draw solution side (*i.e.*, dilutive external concentration polarization). Therefore, the salt content on the membrane surface on the draw solution side deviates from the bulk draw solution, leading to the decrease in salt apparent permeability and the increase in the salt rejection rate.

Fig. 12b shows the effect of the NaCl content in the draw solution on the water permeance. As the NaCl content in the draw solution increases, the overall water flux (J_W) across the membrane increases due to the increase in the driving force, leading to the increase in concentration polarization (*cf.* eq. 9) and thus the decrease in water permeance.

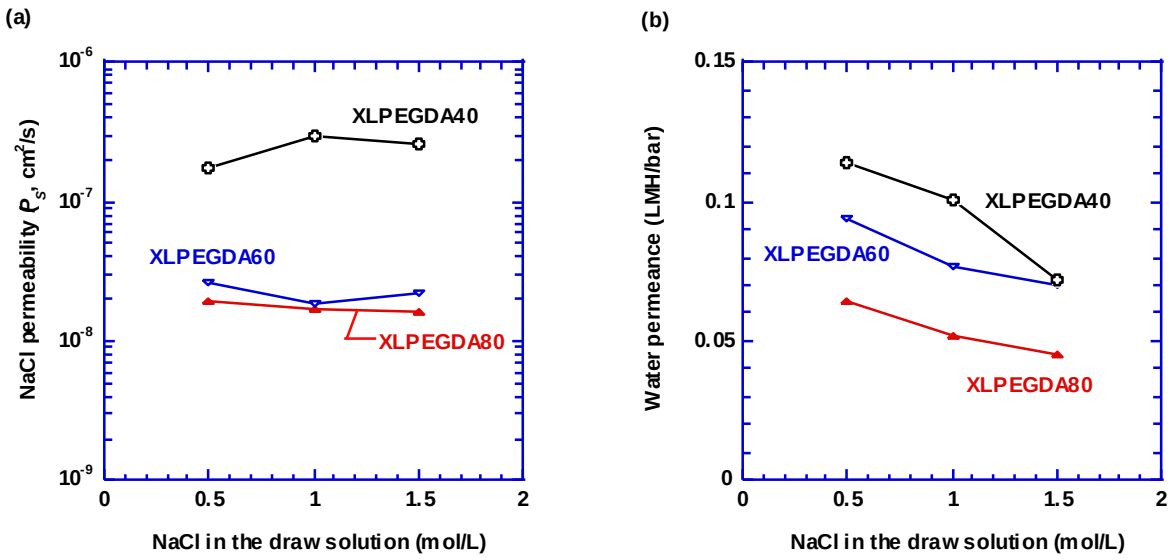

Fig. 12. Effect of the NaCl concentration in the draw solution on (a) the salt permeability and (b) water permeance in the three impregnated membranes based on PEGDA/EtOH.

To elucidate the effect of concentration polarization in the feed side, the IM consisting of XLPEGDA60 was tested with a feed solution containing 0.1 M NaCl and a draw solution containing 1.0 M NaCl. As the feed NaCl content increases from 0 to 0.1 M, the water permeance decreases from 0.0771 LMH/bar to 0.0624 LMH/bar and the salt rejection decreases from 96.8% to 93.9%. This result indicates the external concentration polarization on the feed side of the membrane, presumably because both membrane sides use the same spacer with the same Reynolds number (210). Future work needs to understand the effect of feed and permeate spacer structure in the FO system to reduce the effect of concentration polarization.

CHAPTER 5: DISCUSSIONS

5.1. MODELING OF CONCENTRATION POLARIZATION

For the FO operation in this study, the reverse salt flux to the feed solution only slightly increases the feed salt concentration, due to the large volume of the feed solution. Therefore, the osmotic pressure of the feed solution is negligible compared to that of the draw solution, and the concentration polarization on the feed side of the membrane can be neglected. Eq. 9 can be simplified as [56,68,69]:

$$\ln\left(\frac{J_W + B}{A_W \pi_{D,b} + B}\right) = -\frac{J_W}{k_D} \tag{15}$$

The data from Fig. 12 were represented in Fig. 13, and Eq. 15 was used for modeling. The B values from the kinetic desorption experiments were used here, since these experiments have minimal concentration polarization and yield intrinsic salt permeance. The model fitting is reasonably good, which yields a k_D value of 4.3 LMH or 1.2×10^{-4} cm/s.

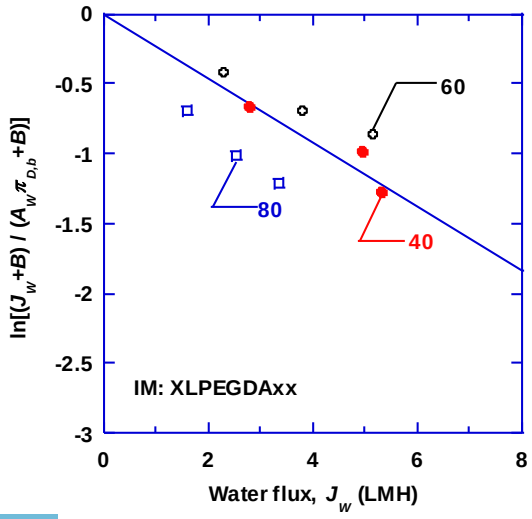

Fig. 13. Correlation of water flux (J_W) with mass transfer coefficient (k_D) in the impregnated membranes for FO applications. The feed is pure water and the draw solution contains 0.5, 1.0 and 1.5 mol/L at 23 ºC. The fitting line is based on Eq. 15 and has a slope of 0.23 LMH^{-1}.

The mass transfer coefficient (k_D) on the surface of flat sheet membranes can be estimated using the film theory. The draw solution in the spacers has a Reynold number of 210 and thus the flow is laminar. The ideal mass transfer coefficient ($k_{D,\text{ideal}}$) can be expressed as [56]:

$$k_{D,\text{ideal}} = 1.62\frac{D_S}{d_h}\left(\frac{v_\infty d_h^{\,2}}{LD_S}\right)^{1/3} = 1.62\left(\frac{D_S^{\,2} v_\infty}{L\cdot 2W}\right)^{1/3} \quad (16)$$

where L (14.6 cm) and W (9.5 cm) is the length and the width of the flow channel in the permeation cell, respectively. The diffusion coefficient of NaCl in the solutions of 0.5 M, 1.0 M and 1.5 M is 1.50×10^{-6} cm^2/s [65]. The $k_{D,\text{ideal}}$ value can be derived and it has a value of 7.7×10^{-4} cm/s, which is higher than the modeled k_D value from the experiments as shown in Fig. 13. This result may not be surprising, considering the effect of spacers on the membrane surfaces. Within the framework of the film theory, the $k_{D,\text{ideal}}$ value can also be used to derive the thickness of the film (δ): $\delta = D_S / k_{D,ideal}$ [15,56]. The δ obtained has a value of 190 μm, which comparable to the spacer thickness (272 μm). The use of permeate carriers with low porosity may have impact on the mass transfer coefficient [70].

5.2. SELECTION OF HYDROPHILIC MATERIALS FOR IMS

Fig. 14 compares the water/NaCl permeation properties in the IMs containing XLPEGDA with other polymers considered for this application. The upper bound is empirically drawn and indicates the highest water/NaCl selectivity achievable for every possible pure water permeability [40]. In general, the IMs prepared in this work shows very high water permeability

and moderate water/NaCl selectivity, though some of the IMs have the separation properties above the upper bound.

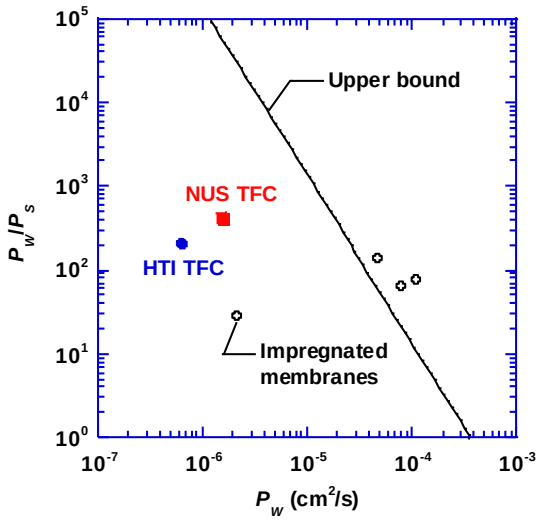

Fig. 14. Correlation between water permeability (P_W, cm^2/s) and water/NaCl permeability selectivity (P_W/P_S). The upper bound line is empirically drawn: $P_W/P_S = 1.4\times10^{-7}/P_W^{\,2}$ [40].

The current state-of-the-art commercial FO membranes exhibit water permeance of 22.9 LMH and reverse salt flux of 6.4 gMH, when tested with pure water as the feed and 1 M NaCl solution as the draw solution [67]. Using the same feed and draw solution, new FO membranes based on cellulose ester substrates at the research stage have been reported to exhibit water permeance as high as 56.9 LMH with the reverse salt flux of 7.8 gMH [21]. Assuming that IMs can be made with a thickness of 10 μm and the external concentration polarization can be eliminated, the IMs should have a water permeability of 6.4×10^{-7} cm^2/s and water/salt selectivity of 210 to match the commercial FO membranes (labeled as HTI TFC in Fig. 14), and a water permeability of 1.6×10^{-6} cm^2/s and 430 to match the TFC based on cellulose ester substrates reported (labeled as NUS TFC). As shown in Fig. 14, these properties are below the upper

bound, and they can be achieved using polymers currently available.

CHAPTER 6: CONCLUSIONS

Current forward osmosis membranes are asymmetric with thick porous support and paper layer, which exhibits significant internal concentration polarization, leading to the low water permeance. This study explores nonporous impregnated membranes consisting of porous polyethylene support impregnated with a highly hydrophilic polymer. A series of well-studied hydrophilic polymers, crosslinked poly(ethylene glycol) (XLPEGDA), are explored in study to illustrate the concept. The impregnated membranes were thoroughly evaluated for water and salt transport properties using three tests, hydraulic dead-end permeation, salt kinetic desorption, and forward osmosis. In general, increasing the solvent content in the prepolymer solution increases water and salt solubility, diffusivity and permeability, and decreases salt rejection, due to the more open structure. In the FO operation, the IMs show water permeance higher than Filmtec SW30, but lower than HTI TFC. On the other hand, these IMs exhibit greater performance ratio than the currently commercial membranes examined such as Filmtec SW30 and HTI TFC, indicating the promise of this new type of membranes for FO applications. Future work will be focused on the mitigation the external concentration polarization for these IMs, such as optimization of the spacer designs, and new impregnated membranes based on polymers with high water permeability and water/NaCl selectivity.

References

[1] M. Elimelech and W. A. Phillip, The future of seawater desalination: energy, technology, and the environment, Science, 333 (2011) 712-717.

[2] R. L. McGinnis and M. Elimelech, Global challenges in energy and water supply: the promise of engineered osmosis, Environ. Sci. Technol., 42 (2008) 8625-8629.

[3] M. A. Shannon, P. W. Bohn, M. Elimelech, J. G. Georgiadis, B. J. Marinas, and A. M. Mayes, Science and technology for water purification in the coming decades, Nature, 452 (2008) 301-310.

[4] L. F. Greenlee, D. F. Lawler, B. D. Freeman, B. Marrot, and P. Moulin, Reverse osmosis desalination: Water sources, technology, and today's challenges, Water Res., 43 (2009) 2317-2348.

[5] G. M. Geise, H. S. Lee, D. J. Miller, B. D. Freeman, J. E. McGrath, and D. R. Paul, Water purification by membranes: The role of polymer science, J. Polym. Sci., Part B: Polym. Phys., 48 (2010) 1685-1718.

[6] A. G. Fane, R. Wang, and M. X. Hu, Synthetic membranes for water purification: status and future, Angew. Chem. Int. Ed., 54 (2015) 3368-3386.

[7] T. Y. Cath, A. E. Childress, and M. Elimelech, Forward osmosis: principles, applications, and recent developments, J. Membr. Sci., 261 (2006) 70-87.

[8] J. C. Su, S. Zhang, M. M. Ling, and T. S. Chung, Forward osmosis: an emerging technology for sustainable supply of clean water, Clean Technol. Envir., 14 (2012) 507-511.

[9] D. L. Shaffer, J. R. Werber, H. Jaramillo, S. H. Lin, and M. Elimelech, Forward osmosis: where are we now?, Desalination, 356 (2015) 271-284.

[10] S. Zhao, L. Zou, C. Y. Tang, and D. Mulcahy, Recent developments in forward osmosis: opportunities and challenges, J. Membr. Sci., 396 (2012) 1-21.

[11] T. S. Chung, X. Li, R. C. Ong, Q. C. Ge, H. L. Wang, and G. Han, Emerging forward osmosis (FO) technologies and challenges ahead for clean water and clean energy applications, Current Opinion in Chemical Engineering, 1 (2012) 246-257.

[12] J. R. McCutcheon, R. L. McGinnis, and M. Elimelech, Desalination by ammonia–carbon dioxide forward osmosis: influence of draw and feed solution concentrations on process performance, J. Membr. Sci., 278 (2006) 114-123.

[13] Q. P. Zhao, N. P. Chen, D. L. Zhao, and X. M. Lu, Thermoresponsive magnetic nanoparticles for seawater desalination, ACS Appl. Mater. Interfaces, 5 (2013) 11453-11461.

[14] R. J. Petersen, Composite reverse-osmosis and nanofiltration membranes, J. Membr. Sci., 83 (1993) 81-150.

[15] J. R. McCutcheon and M. Elimelech, Influence of concentrative and dilutive internal concentration polarization on flux behavior in forward osmosis, J. Membr. Sci., 284 (2006) 237-247.

[16] J. R. McCutcheon and M. Elimelech, Influence of membrane support layer hydrophobicity on water flux in osmotically driven membrane processes, J. Membr. Sci., 318 (2008) 458-466.

[17] K. L. Lee, R. W. Baker, and H. K. Lonsdale, Membranes for power generation by pressure-retarded osmosis, J. Membr. Sci., 8 (1981) 141-171.

[18] H. Lin, S. M. Thompson, A. Serbanescu-Martin, H. G. Wijmans, K. D. Amo, K.

Lokhandwala, and T. C. Merkel, Dehydration of natural gas using membranes. Part I: composite membranes, J. Membr. Sci., 413-414 (2012) 70-81.
[19] R. W. Baker, Membrane Technology and Applications, 3rd ed., John Wiley and Sons, Ltd., Chichester, UK, 2012.
[20] J. T. Arena, B. McCloskey, B. D. Freeman, and J. R. McCutcheon, Surface modification of thin film composite membrane support layers with polydopamine: enabling use of reverse osmosis membranes in pressure retarded osmosis, J. Membr. Sci., 375 (2011) 55-62.
[21] R. C. Ong, T. S. Chung, J. S. de Wit, and B. J. Helmer, Novel cellulose ester substrates for high performance flat-sheet thin-film composite (TFC) forward osmosis (FO) membranes, J. Membr. Sci., 473 (2015) 63-71.
[22] B. Nhu-Ngoc, M. L. Lind, E. M. V. Hoek, and J. R. McCutcheon, Electrospun nanofiber supported thin film composite membranes for engineered osmosis, J. Membr. Sci., 385 (2011) 10-19.
[23] X. Song, Z. Liu, and D. D. Sun, Nano gives the answer: breaking the bottleneck of internal concentration polarization with a nanofiber composite forward osmosis membrane for a high water production rate, Adv. Mater., 23 (2011) 3256-3260.
[24] F. Q. Liu, B. L. Yi, D. M. Xing, J. R. Yu, and H. M. Zhang, Nafion/PTFE composite membranes for fuel cell applications, J. Membr. Sci., 212 (2003) 213-223.
[25] K. H. Kim, S. Y. Ahn, I. H. Oh, H. Y. Ha, S. A. Hong, M. S. Kim, Y. Lee, and Y. C. Lee, Characteristics of the Nafion - impregnated polycarbonate composite membranes for PEMFCs, Electrochim. Acta, 50 (2004) 577-581.
[26] J. H. Shim, I. G. Koo, and W. M. Lee, Nafion-impregnated polyethylene-terephthalate film used as the electrolyte for direct methanol fuel cells, Electrochim. Acta, 50 (2005) 2385-2391.
[27] M. H. Yildirim, D. Stamatialis, and M. Wessling, Dimensionally stable Nafion-polyethylene composite membranes for direct methanol fuel cell applications, J. Membr. Sci., 321 (2008) 364-372.
[28] T. Yamaguchi, H. Hayashi, S. Kasahara, and S. Nakao, Plasma-graft pore-filling electrolyte membranes using a porous poly(tetrafluoroethylene) substrate, Electrochem., 70 (2002) 950-952.
[29] T. Yamaguchi, F. Miyata, and S. Nakao, Polymer electrolyte membranes with a pore-filling structure for a direct methanol fuel cell, Adv. Mater., 15 (2003) 1198-1201.
[30] T. Yamaguchi, F. Miyata, and S. Nakao, Pore-filling type polymer electrolyte membranes for a direct methanol fuel cell, J. Membr. Sci., 214 (2003) 283-292.
[31] M. H. Yildirim, A. Schwarz, D. F. Stamatialis, and M. Wessling, Impregnated membranes for direct methanol fuel cells at high methanol concentrations, J. Membr. Sci., 328 (2009) 127-133.
[32] M. J. Lee, J. H. Kim, H. S. Lim, S. Y. Lee, H. K. Yu, J. H. Kim, J. S. Lee, Y. K. Sun, M. D. Guiver, K. Do Suh, and Y. M. Lee, Highly lithium-ion conductive battery separators from thermally rearranged polybenzoxazole, Chem. Commun., 51 (2015) 2068-2071.
[33] S. S. Zhang, A review on the separators of liquid electrolyte Li-ion batteries, J. Power Sources, 164 (2007) 351-364.
[34] A. D. Mossman, Membrane exchange humidifier for a fuel cell, US Patent 6864005 B2, 2005.
[35] A. D. Mossman, Method for humidifying a reactant stream for a fuel cell, U.S. Patent

7784770 B2, 2010.
[36] R. Huizing, W. Merida, and F. Ko, Impregnated electrospun nanofibrous membranes for water vapour transport applications, J. Membr. Sci., 461 (2014) 146-160.
[37] H. Lin, S. M. Thompson, A. Serbanescu-Martin, J. G. Wijmans, K. D. Amo, K. A. Lokhandwala, B. Low, and T. C. Merkel, Dehydration of natural gas using membranes. Part II: sweep/countercurrent design and field test, J. Membr. Sci., 432 (2013) 106-114.
[38] J. G. Wijmans and R. W. Baker, The solution-diffusion model: a review, J. Membr. Sci., 107 (1995) 1-21.
[39] D. R. Paul, Reformulation of the solution-diffusion theory of reverse osmosis, J. Membr. Sci., 241 (2004) 371-386.
[40] G. M. Geise, H. B. Park, A. C. Sagle, B. D. Freeman, and J. E. McGrath, Water permeability and water/salt selectivity tradeoff in polymers for desalination, J. Membr. Sci., 369 (2011) 130-138.
[41] R. F. Probstein, Physicochemical hydrodynamics: an introduction, John Wiley & Sons, 2005.
[42] N. Y. Yip, A. Tiraferri, W. A. Phillip, J. D. Schiffrnan, L. A. Hoover, Y. C. Kim, and M. Elimelech, Thin-film composite pressure retarded osmosis membranes for sustainable power generation from salinity gradients, Environ. Sci. Technol., 45 (2011) 4360-4369.
[43] J. G. Wijmans, S. Nakao, and C. A. Smolders, Flux limitation in ultrafiltration: osmotic pressure model and gel layer model, J. Membr. Sci., 20 (1984) 115-124.
[44] J. G. Wijmans, A. L. Athayde, R. Daniels, J. H. Ly, H. D. Kamaruddin, and I. Pinnau, The role of boundary layers in the removal of volatile organic compounds from water by pervaporation, J. Membr. Sci., 109 (1996) 135-146.
[45] U. Beuscher and C. H. Gooding, The influence of the porous support layer of composite membranes on the separation of binary gas mixtures, J. Membr. Sci., 152 (1999) 99-116.
[46] N. Y. Yip, A. Tiraferri, W. A. Phillip, J. D. Schiffman, and M. Elimelech, High performance thin-film composite forward osmosis membrane, Environ. Sci. Technol., 44 (2010) 3812-3818.
[47] H. Lin, T. Kai, B. D. Freeman, S. Kalakkunnath, and D. S. Kalika, The effect of cross-linking on gas permeability in crosslinked poly(ethylene glycol diacrylate), Macromolecules, 38 (2005) 8381-8393.
[48] H. Lin, E. Van Wagner, S. J. Swinnea, B. D. Freeman, S. J. Pas, A. J. Hill, S. Kalakkunnath, and D. S. Kalika, Transport and structural characteristics of crosslinked poly(ethylene oxide) rubbers, J. Membr. Sci., 276 (2006) 145-161.
[49] H. Ju, B. D. McCloskey, A. C. Sagle, Y. H. Wu, V. A. Kusuma, and B. D. Freeman, Crosslinked poly(ethylene oxide) fouling resistant coating materials for oil/water separation, J. Membr. Sci., 307 (2008) 260-267.
[50] H. Ju, A. C. Sagle, B. D. Freeman, J. I. Mardel, and A. J. Hill, Characterization of sodium chloride and water transport in crosslinked poly(ethylene oxide) hydrogels, J. Membr. Sci., 358 (2010) 131-141.
[51] H. B. Park, B. D. Freeman, Z. B. Zhang, M. Sankir, and J. E. McGrath, Highly chlorine-tolerant polymers for desalination, Angew. Chem. Int. Ed., 47 (2008) 6019-6024.
[52] Y.-H. Wu, H. B. Park, T. Kai, B. D. Freeman, and D. S. Kalika, Water uptake, transport and structure characterization in poly(ethylene glycol) diacrylate hydrogels, J. Membr. Sci., 347 (2010) 197-208.
[53] A. C. Sagle, H. Ju, B. D. Freeman, and M. M. Sharma, PEG-based hydrogel membrane

coatings, Polymer, 50 (2009) 756-766.
[54] H. Yasuda, C. E. Lamaze, and L. D. Ikenberry, Permeability of solutes through hydrated polymer membranes. Part I. diffusion of sodium chloride, Macromol. Chem. Phys., 118 (1968) 19-35.
[55] T. Y. Cath, M. Elimelech, J. R. McCutcheon, R. L. McGinnis, A. Achilli, D. Anastasio, A. R. Brady, A. E. Childress, I. V. Farr, and N. T. Hancock, Standard methodology for evaluating membrane performance in osmotically driven membrane processes, Desalination, 312 (2013) 31-38.
[56] E. M. V. Hoek, A. S. Kim, and M. Elimelech, Influence of crossflow membrane filter geometry and shear rate on colloidal fouling in reverse osmosis and nanofiltration separations, Environ. Eng. Sci., 19 (2002) 357-372.
[57] E. M. Van Wagner, A. C. Sagle, M. M. Sharma, and B. D. Freeman, Effect of crossflow testing conditions, including feed pH and continuous feed filtration, on commercial reverse osmosis membrane performance, J. Membr. Sci., 345 (2009) 97-109.
[58] H. Yasuda, L. Ikenberry, and C. Lamaze, Permeability of solutes through hydrated polymer membranes. Part II. permeability of water soluble organic solutes, Macromol. Chem. Phys., 125 (1969) 108-118.
[59] K. Nagai, S. Tanaka, Y. Hirata, T. Nakagawa, M. E. Arnold, B. D. Freeman, D. Leroux, D. E. Betts, J. M. DeSimone, and F. A. DiGiano, Solubility and diffusivity of sodium chloride in phase-separated block copolymers of poly (2-dimethylaminoethyl methacrylate), poly (1, 1′ -dihydroperfluorooctyl methacrylate) and poly (1, 1, 2, 2-tetrahydroperfluorooctyl acrylate), Polymer, 42 (2001) 09941-09948.
[60] H. Lin and B. D. Freeman, Permeation and diffusion, in H. Czichos, L. E. Smith and T. Saito (Eds.), Springer-Handbook of Materials Measurement Methods, Springer, 2006, pp. 371-387.
[61] G. M. Geise, D. R. Paul, and B. D. Freeman, Fundamental water and salt transport properties of polymeric materials, Prog. Polym. Sci., 39 (2014) 1-42.
[62] H. Yasuda, C. Lamaze, and A. Peterlin, Diffusive and hydraulic permeabilities of water in water‐swollen polymer membranes, J. Polym. Sci., Part A: Polym. Chem., 9 (1971) 1117-1131.
[63] O. Okay, Macroporous copolymer networks, Prog. Polym. Sci., 25 (2000) 711-779.
[64] A. Chomff, A. Chomff, and S. Newman, Polymer networks: Structure and mechanical properties, Plenum Press, New York, (1971).
[65] V. M. M. Lobo, Mutual diffusion-coefficients in aqueous-electrolyte solutions (technical report), Pure Appl. Chem., 65 (1993) 2614-2640.
[66] V. Hervouet, HTI starts producing thin-film composite FO membrane, Membr. Techn., 2012 (2012) 5-6.
[67] J. Ren and J. R. McCutcheon, A new commercial thin film composite membrane for forward osmosis, Desalination, 343 (2014) 187-193.
[68] C. Y. Y. Tang, Q. H. She, W. C. L. Lay, R. Wang, and A. G. Fane, Coupled effects of internal concentration polarization and fouling on flux behavior of forward osmosis membranes during humic acid filtration, J. Membr. Sci., 354 (2010) 123-133.
[69] R. Wang, L. Shi, C. Y. Y. Tang, S. R. Chou, C. Qiu, and A. G. Fane, Characterization of novel forward osmosis hollow fiber membranes, J. Membr. Sci., 355 (2010) 158-167.
[70] M. Park and J. H. Kim, Numerical analysis of spacer impacts on forward osmosis membrane process using concentration polarization index, J. Membr. Sci., 427 (2013) 10-

20.